IGARSS 2021 - 2021 IEEE International Geoscience and Remote Sensing Symposium | 978-1-6654-0369-6/21/$31.00 ©2021 IEEE | DOI: 10.1109/IGARSS47720.2021.9553158

POLARIMETRIC SAR IMAGES FOR CHARACTERIZATION OF URBAN TARGETS

Hossein Aghababaei[1], Giampaolo Ferraioli[2] and Roghayeh Zamani[2]

[1]Department of Earth Observation Science, University of Twente Faculty of Geo-Information Science and Earth Observation, Twente, Netherlands
[2]Dipartimento di Scienze e Tecnologie, Università degli Studi di Napoli "Parthenope", Naples, Italy

ABSTRACT

This paper addresses the 3D classification of superimposed target scattering mechanisms in polarimetric synthetic aperture radar (SAR) images of urban environments. Theoretically, the solution of this problem is possible with polarimetric tomographic SAR focusing techniques. In this work, we investigate how SAR Tomography (TomoSAR) can be used to identify and distinguish the superimposed target mechanisms. In particular, various strategies are employed to separate and characterize the polarimetric scattering patterns of targets in layover regions. Extensive and comparative analyses are performed to answer how accurately different strategies can identify the polarimetric scattering pattern.

Index Terms— 3D classification, Decomposition, SAR tomography.

1. INTRODUCTION

Polarimetric synthetic aperture radar (SAR) remote sensing has been used as a powerful tool for monitoring the Earth's surface, especially for creating the map to classify land use and land cover in a complex urban environment [1, 2]. In the context of classification of polarimetric SAR (PolSAR) images and depending on whether reference data are used (i.e., supervised scheme) or not (i.e., unsupervised scheme), many efficient techniques have been used to assign each pixel of PolSAR data to a particular land use/land cover or backscatter mechanism [3-8].

Over the complex urban scenario, various scattering mechanisms, including odd-bounce scattering from rooftops and from the ground, double-bounce scattering due to wall-ground reflections, and volumetric scattering over vegetated urban areas due to geometric distortion or layover phenomenon can fall into a single SAR resolution cell. Such a problem poses a serious limitation to the classification and characterization of pixels with the conventional PolSAR classifiers, forcing the classification to be performed in two-dimensional space with azimuth-range domain.

To achieve the goal of 3D classification, 3D image reconstruction of urban environments with the backscattering mechanisms is required. SAR Tomography (TomoSAR) with resolution capability in the height dimension is a natural solution for 3D backscatter reconstruction of urban environments; where TomoSAR forms an additional synthetic aperture in the height direction using multiple SAR images. This 3D imaging technique is now widely used in remote sensing of complex urban environments. [5-7].

The availability of polarization information can increase the synthesis performance and allows to describe the electromagnetic behavior of illuminated objects located in a resolution cell but at different heights. Polarimetric TomoSAR techniques are therefore of great interest. In [8, 9] a different overview of TomoSAR reconstruction was given, allowing the estimation of full-rank polarimetric features of the superimposed scatterers. The studies provided the polarimetric versions of conventional tomographic reconstruction techniques such as beamforming, Capon, Multiple Signal Classification (MUSIC) to improve the height estimation of buildings and estimate their scattering patterns. In addition, model adaptive polarimetric Noise Subspace Fitting (NSF) was used to overcome the possible limitations of statistical adaptivity of the above approaches. The experiments clearly showed that the polarimetric NSF outperforms other polarimetric estimators (Capon and MUSIC) in locating deterministic scatterers. Although the performance of the methods used in the reconstruction of reflectivity and height estimation has been evaluated and assessed, a more in-depth evaluation of the methods in relation to the reconstruction of the polarimetric backscattering pattern is still needed.

In order to answer the question of how reliable the estimated scattering patterns from polarimetric data are, an attempt has been made in this paper to evaluate different approaches in terms of the estimated backscattering pattern of the overlaid targets. In particular, three different strategies are considered. The first strategy decomposes and characterizes the polarimetric scattering patterns using the concept of the conventional decomposition framework [10], while the second strategy is based on the separation of the superimposed scattering mechanisms using tomographic reconstruction. Furthermore, the efficiency of a mixed strategy based on decomposition and reconstruction, as third strategy, is also evaluated. In summary, the results of this

study shed light on how reliable the estimated scattering information from different strategies is in target identification. The framework is applied to polarimetric multi-baseline data stacks acquired in L-band by Jet Propulsion Laboratory (JPL) with the Uninhabited Aerial Vehicle SAR (UAVSAR) over l'Amitié stadium in Gabon.

2. POLARIMETRIC SAR DATA

It is generally known that the polarization information contained in the waves backscattered from the scene is related to the geometric structure and orientation as well as the structures of the observed objects. In particular, radar polarimetry exploits the fully vectorial nature of polarized EM signals; by impinging a wave on an object, the aforementioned characteristic target information can be represented in a 2 × 2 scattering matrix, **S**. In the case of horizontally (h) or vertically (v) polarized antennas and at the basis of (h, v), the full polarimetric response of the target in a specific azimuth range resolution cell can be given by

$$\mathbf{S} = \begin{bmatrix} y_{hh} & y_{hv} \\ y_{vh} & y_{vv} \end{bmatrix} \tag{1}$$

where the complex scattering coefficient y_{pq}, indexed as p and q represents the EM signal and is transmitted over the polarization channel q and received on the channel p. When the roles of the transmitting and receiving antennas are reversed, as in the reciprocity theorem, the scattering matrix is symmetric, i.e., $y_{hv} = y_{vh}$.

In the polarimetric SAR (PolSAR), **S** can be vectorized as the Pauli target scattering vector **k** given by

$$\mathbf{k} = \frac{1}{\sqrt{2}} \begin{bmatrix} y_{hh} + y_{vv} \\ y_{hh} - y_{vv} \\ 2y_{hv} \end{bmatrix} \tag{2}$$

The overall process of deterministic scatterers can be described by **k**, while for the naturally distributed scatterers present in forested areas, the target vectors may follow a random property if the wavelength of the SAR system is smaller than that of the resolution cell. For this case, the target vectors can be modeled by the complex circular Gaussian probability density function, where the second-order statistics can be represented by the polarimetric coherence matrix $\mathbf{T} = E\{\mathbf{k}\mathbf{k}^{\dagger}\}$.

3. TARGET SCATTERING DECOMPOSITION

In the treatment of a single polarimetric SAR image, decomposition is a method that acts on the backscattering to identify and isolate different scattering mechanisms [10]. Two main classes of decomposition can be identified: 1) coherent decomposition, developed to characterize fully polarized scattered waves for which the fully polarimetric information is contained in the scattering matrix; 2) incoherent decomposition, used to characterize partially polarized waves for which the fully polarimetric information can only be represented by the Mueller, covariance or coherence matrices. In general, conventional averaging and statistical methods are applied to PolSAR images; therefore, incoherent approaches are often chosen for postprocessing.

4. POLARIMETRIC SAR TOMOGRAPHY

Considering an azimuth-range resolution cell in the polarimetric SAR image containing L scatterers located at different elevations, the polarimetric data vector measured by a multi-baseline TomoSAR configuration over N acquisition in three linear polarization channels (HH, HV, and VV, i.e., in Pauli representation) can be represented $\mathbf{y} \in \mathbb{C}^{3N\times 1}$ by [9]:

$$\mathbf{y} = \sum_{l=1}^{L} \mathbf{B}_{\mathbf{a}}(z_l)\mathbf{k}_l s_l + \mathbf{n} = \mathbf{A}(\mathbf{z},\mathbf{K})\mathbf{s} + \mathbf{n} \tag{3}$$

where s_l and $\mathbf{k_l}$ is the realization of complex backscattering and polarimetric pattern of the l^{th} scatterer, and the polarimetric steering vector $\mathbf{a}(z_l,\mathbf{k_l})$ and steering matrix $\mathbf{A}(\mathbf{z},\mathbf{K})$ are represented as:

$$\begin{aligned} \mathbf{a}(z_l,\mathbf{k}_l) &= \left(\mathbf{I}_{3\times 3} \otimes \mathbf{a}(z_l)\right)\mathbf{k}_l = \mathbf{B}_{\mathbf{a}}(z_l)\mathbf{k}_l \\ \mathbf{A}(\mathbf{z},\mathbf{K}) &= [\mathbf{a}(z_1,\mathbf{k}_1),.....,\mathbf{a}(z_L,\mathbf{k}_L)] \end{aligned} \tag{4}$$

with **z** and **K** the parameters of unknown source heights and unknown polarimetric scattering pattern, $\mathbf{I_{3\times 3}}$ is 3×3 identity matrix and ⊗ denotes the Kronecker product. From the assumption of having additive white noise in space and time **n**, with gaussian distribution and zero mean and standard deviation of σ_n^2, the covariance matrix of polarimetric data vector in (1) can be given by:

$$\mathbf{R} = \sum_{l=1}^{L} \mathbf{T_3}(z_l) \otimes \mathbf{a}(z_l)\mathbf{a}^{\dagger}(z_l) + \sigma_n^2\mathbf{I} \quad \in \mathrm{C}^{3N\times 3N} \tag{5}$$

where $\mathbf{T}(z_l) = E[|s_l|^2\mathbf{k_l}\mathbf{k_l}^{\dagger}]$ describes polarimetric coherence matrix of the l^{th} scatterer.

Polarimetric tomographic reconstruction consists in estimating the polarimetric coherence matrix of L observed sources. The estimation of the above matrix can be performed using various spectral estimation techniques. Similar to the reconstruction of reflectivity from single polarization, the results of fully polarimetric reconstruction using polarimetric beamforming and Capon are robust to artifacts but have coarse resolution, while polarimetric Capon can achieve higher resolution with considerable signal-to-noise ratio (SNR). Fully polarimetric MUSIC and subspace fitting methods can improve resolution and sidelobe level, while NSF can outperform other polarimetric techniques in terms of resolution and localization of deterministic scatterers. The final solutions of the commonly adapted Capon approach is given as [9]:

$$\mathbf{T}(z_l) = \left(\mathbf{B}_{\mathbf{a}}^{\dagger}(z_l)\,\hat{\mathbf{R}}\,\mathbf{B}_{\mathbf{a}}(z_l)\right)^{-1} \tag{6}$$

where $\hat{\mathbf{R}}$ is the polarimetric sample covariance matrix estimated over the spatial neighborhood of pixel of interest.

5. MULTI-BASELINE DECOMPOSITION

In addition to the effectiveness of the reconstruction algorithm, the separation and characterization of the superimposed scatterers strongly depends on the configuration of the MB SAR sensor. Typically, decomposition is an alternative approach that can provide a promising solution in separating the scattering mechanisms. With respect to polarimetric MB data, several processing strategies have been presented in the literature [11-13]; a widely used approach is the sum of Kronecker products (SKP) [13], which forms the basis for decomposing MB data from a forested area along the elevation direction. The method models polarimetric radar backscattering from the ground and canopy layers in forested areas. Using the SKP, the multi-baseline polarimetric covariance matrix (**R**) can be expressed by the Kronecker product between two matrices:

$$\mathbf{R_p} = \sum_{q=1}^{2} \tilde{\mathbf{B}}_{\mathbf{q}} \otimes \tilde{\mathbf{C}}_{\mathbf{q}} \tag{7}$$

where $\tilde{\mathbf{C}}_q$ and $\tilde{\mathbf{B}}_q$ account for the correlation among different polarizations and baselines, respectively. It has been shown that the matrices $\tilde{\mathbf{C}}_q$ and $\tilde{\mathbf{B}}_q$ are related to the polarimetric signatures ($\mathbf{C}_1$, C_2) and interferometric structure matrices ($\mathbf{R}_1$, $\mathbf{R}_2$) of the ground and canopy via a linear invertible transformation:

$$\begin{aligned} \mathbf{R}_1 &= a\tilde{\mathbf{B}}_p + (1-a)\tilde{\mathbf{B}}_q, \quad \mathbf{C}_1 = \frac{1}{a-b}\left((1-b)\tilde{\mathbf{C}}_p - b\tilde{\mathbf{C}}_q\right) \\ \mathbf{R}_2 &= b\tilde{\mathbf{B}}_p + (1-b)\tilde{\mathbf{B}}_q, \quad \mathbf{C}_2 = \frac{1}{a-b}\left(-(1-a)\tilde{\mathbf{C}}_p + a\tilde{\mathbf{C}}_q\right) \end{aligned} \tag{8}$$

where (a, b) are two real numbers that were obtained by requiring the semi-positive definitiveness condition for the above four matrices.

In this paper, the idea is to evaluate polarimetric scattering pattern estimation using:

I) conventional decomposition technique explained in Section 3,

II) polarimetric reconstruction presented in Section 4,

II) multi-baseline decomposition given in section 5

3. EXPERIMENTS

Real dataset experiments are performed with 9 stacks of UAVSAR L-band full polarimetric datasets acquired in March 2016 over l'Amitié stadium in Gabon. The total baseline is about 25 m and the azimuth range resolution is 1.1×1.67 m. Fig. 1(a) shows the Pauli color composite of the master image.

To gain an understanding on the efficiency of the approaches considered, tomographic and conventional decomposition techniques are implemented and their results are later used to produce a classified image. The classification results are provided using the conventional H-α-Wishart classifier and compared with the 3D classification framework. Fig. 1(b) represents the 2D classified image of the study area. In the H-α-Wishart classifier framework, the H-α decomposition theorem [10] is used to provide an initial estimate of the pixel distribution into the classes, which produces better convergence of the unsupervised classification algorithm. Starting from the initial clusters and within the iteration process, the cluster merging process continues based on the Wishart distance estimated using the coherence matrix of each pixel and the coherence matrices of the clusters. The 8 clusters generated are associated with 8 zones in the H-α plane, where the zones are explained by 1) complex structure, 2) random anisotropic scatterers, 4) double reflection propagation effects, 5) anisotropic particles, 6) random surface, 7) dihedral reflector, 8) dipole, and 9) Bragg surface scattering.

From the 2D classified image, it can be seen that the pitch and vegetation areas are mainly recognized by random surface and anisotropic scattering, while the running track in the stadium and bare areas are labeled as zones 1 and 2. Surface scattering is seen over the platform and some infrastructures, dihedral scattering is also seen over the roof of the stadium.

From the classified map in Fig. 1(b), it can be seen that the 2D classification is not able to identify and separate the scattering mechanisms falling into a resolution cell. For the 3D classification, the H-α-Wishart classifier is performed in the polarimetric coherence matrix T3 reconstructed by the polarimetric Capon algorithm. To allow a fair comparison, the classifier is first applied only to the height position of the dominant scatterer, which is justified by the peak of the height signal of the span image. Fig. 1(c) shows the classified map of the dominant scatterers. As can be seen in Fig. 1(c), dihedral reflections mainly occur due to the wave interaction between the ground and the platforms, while here the platform is mainly classified as zone 4 and 7, and the bare region is classified as zone 1 and 2. The main difference between the results of the dominant scatterers of T3 and the 2D classifier in Fig. 1(c) is observed in the vegetation areas and the playing field of the stadium, where, due to the overestimation of the α-angle reconstructed by Capon, parts of the playing field with double reflection are identified in zone 4, it was previously identified as a random area in Fig. 1(b). Obviously, the acquisition parameters of the MB dataset may affect the reliability of the reconstructed T3.

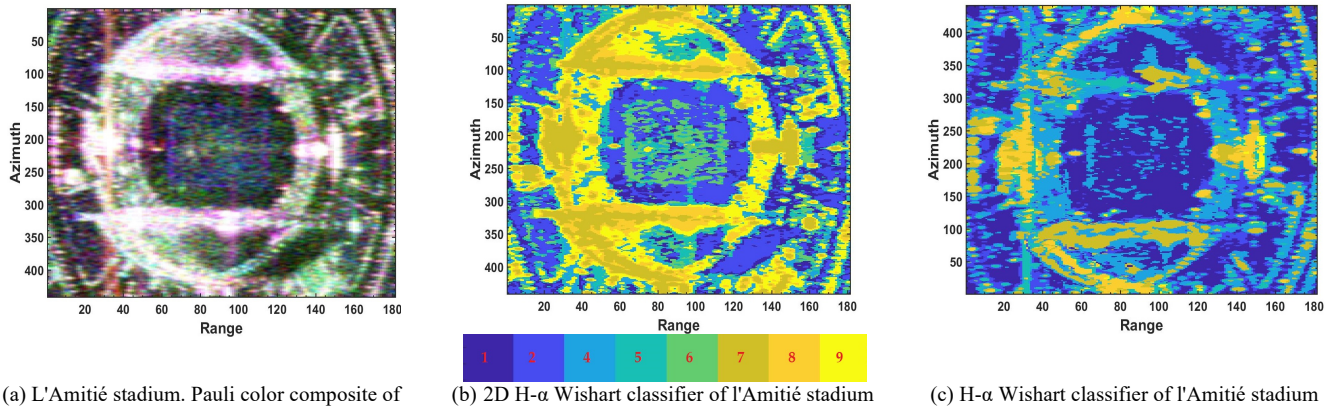

(a) L'Amitié stadium. Pauli color composite of master image. by UAVSAR

(b) 2D H-α Wishart classifier of l'Amitié stadium

(c) H-α Wishart classifier of l'Amitié stadium using Capon based full-rank reconstruction of **T**.

Fig.1 Experimental results

REFERENCES

[1] L. Jong-Sen, M. R. Grunes, and E. Pottier, "Quantitative comparison of classification capability: fully polarimetric versus dual and single-polarization SAR," *IEEE Transactions on Geoscience and Remote Sensing,* vol. 39, no. 11, pp. 2343-2351, 2001

[2] T. M. Pellizzeri, P. Gamba, P. Lombardo, and F. Dell'Acqua, "Multitemporal/multiband SAR classification of urban areas using spatial analysis: statistical versus neural kernel-based approach," *IEEE Transactions on Geoscience and Remote Sensing,* vol. 41, no. 10, pp. 2338-2353, 2003

[3] H. Aghababaee and M. R. Sahebi, "Game theoretic classification of polarimetric SAR images," *European Journal of Remote Sensing,* vol. 48, no. 1, pp. 33-48, 2015.

[4] L. Ferro-Famil, E. Pottier, and L. Jong-Sen, "Unsupervised classification of multifrequency and fully polarimetric SAR images based on the H/A/Alpha-Wishart classifier," *IEEE Transactions on Geoscience and Remote Sensing,* vol. 39, no. 11, pp. 2332-2342, 2001

[5] H. Aghababaee, A. Budillon, G. Ferraioli, V. Pascazio, and G. Schirinzi, "Full 3D DEM Generation in Urban Area By Improving Estimation from SAR Tomography," in *IGARSS 2018 - 2018 IEEE International Geoscience and Remote Sensing Symposium*, 2018, pp. 6087-6090

[6] H. Aghababaei, A. Budillon, G. Ferraioli, A. C. Johnsy, V. Pascazic, and G. Schirinzi, "Multiple Scatterers Detection Based on Signal Correlation Eploitation in Urban Sar Tomography," in *IGARSS 2018 - 2018 IEEE International Geoscience and Remote Sensing Symposium*, 22-27 July 2018, pp. 8691-8694, 2018

[7] X. X. Zhu and R. Bamler, "Demonstration of Super-Resolution for Tomographic SAR Imaging in Urban Environment," *IEEE Transactions on Geoscience and Remote Sensing,* vol. 50, no. 8, pp. 3150-3157, 2012

[8] L. Ferro-Famil, Y. Huang, and S. Tebaldini, "Polarimetric characterization of 3-D scenes using high-resolution and Full-Rank Polarimetric tomographic SAR focusing," in *2016 IEEE International Geoscience and Remote Sensing Symposium (IGARSS)*, 10-15 July 2016 2016, pp. 5694-5697

[9] Y. Huang, L. Ferro-Famil, and A. Reigber, "Under-Foliage Object Imaging Using SAR Tomography and Polarimetric Spectral Estimators," *IEEE Transactions on Geoscience and Remote Sensing,* vol. 50, no. 6, pp. 2213-2225, 2012

[10] S. R. Cloude and E. Pottier, "A review of target decomposition theorems in radar polarimetry," *IEEE Transactions on Geoscience and Remote Sensing,* vol. 34, no. 2, pp. 498-518, 1996.

[11] H. Aghababaee and M. R. Sahebi, "Model-based target scattering decomposition of polarimetric SAR tomography," *IEEE Transactions on Geoscience and Remote Sensing,* vol. 56, no. 2, pp. 972-983, 2017.

[12] M. Neumann, L. Ferro-Famil, and A. Reigber, "Estimation of forest structure, ground, and canopy layer characteristics from multibaseline polarimetric interferometric SAR data," *IEEE Transactions on Geoscience and Remote Sensing,* vol. 48, no. 3, pp. 1086-1104, 2009.

[13] S. Tebaldini, "Algebraic synthesis of forest scenarios from multibaseline PolInSAR data," *IEEE Transactions on Geoscience and Remote Sensing,* vol. 47, no. 12, pp. 4132-4142, 2009.